A Generalized Per-phase Equivalent Circuit Model of the PMSM with Predictable Core Loss

Xin Ba, Xiaodong Sun, *Senior Member, IEEE*, Zhenjie Gong, Youguang Guo, *Senior Member, IEEE*, Chengning Zhang, and Jianguo Zhu, *Senior Member, IEEE*

***Abstract*— Equivalent circuit model (ECM) of the permanent magnet (PM) synchronous motor (PMSM) lays the foundation of the motor analysis, design, optimization, and control. However, the most widely used ECM of the PMSM ignores the core loss, which accounts for a considerable part of the electromagnetic loss and may exceed the copper loss in the medium and high-speed ranges. Previous researches of ECMs with predictable core loss are hard to satisfy the prediction precision over a broad range of speed and current. Therefore, a generalized per-phase ECM of the PMSM with predictable core loss is proposed. The proposed ECM topology and parameter identification method can effectively enhance the prediction accuracy of both the no-load and load core loss, and each component of the core loss in terms of the hysteresis, eddy current, and anomalous loss can be analyzed separately. Apart from the core loss, the proposed ECM has better precision in predicting the motor's output performance, such as mechanical characteristics, compared with traditional ECMs. The merits of the proposed ECM have been experimentally validated on the prototype of a PM transverse flux synchronous motor. This proposed ECM can be promotionally employed in other control strategies, such as model predictive control, to improve the PMSM performance.**

***Index Terms*—Core loss, equivalent electric circuit model, magnetic saturation effect, permanent magnet synchronous motor (PMSM), transverse flux synchronous motor.**

I. Introduction

EQIVALENT circuit model (ECM) of the motor which equals the mathematical models lays the foundation of the motor analysis, design, optimization, and control. Since the rotor of the synchronous motor rotates at the synchronous speed, i.e., the speed of the rotating magnetic field of the stator, the electromagnetic properties of the rotor are eliminated in the ECM, resulting in a more straightforward topology and easy-understanding physical significance compared to that of the asynchronous motor. In recent decades, benefiting from the vigorous development of rare earth permanent magnet (PM) materials, the permanent magnet synchronous motor (PMSM) with low copper loss, high efficiency, high power density and torque density has achieved a wide range of applications and research [1-6], especially in the electric vehicles (EVs), hybrid electric vehicles (HEVs) [7-9], and unmanned aerial vehicles [10]. Among many types of PMSMs, PM transverse flux synchronous motors (TFSMs) have attracted strong interest in research and industry applications due to their unique features like high torque density capability and simple winding structure [11-15]. Because this kind of motor has a complex configuration with three-dimensional (3D) magnetic flux path, the soft magnetic composite (SMC) material is selected to press the stator, which is very difficult to use the steel sheet as the stator of the TFSM [14-17]. In the SMC machine, the core loss takes a significant part of power loss. Therefore, while this study focuses on the ECM of the PMSM, the PM TFSM prototype is employed to validate the proposed method.

There are two main electromagnetic loss in the PMSM, i.e., the core loss and copper loss [18, 19]. The core loss increases significantly with the motor speed, and exceeds the copper loss and becomes the dominant component of the electromagnetic loss when the motor operates in the medium and high-speed ranges [20, 21]. However, in the traditional ECM or mathematical models of the PMSM, the core loss is neglected [22-25], resulting in large calculation errors and limited application in high-speed and high-torque/power density PMSM performance calculation. Although some scholars have engaged in core loss modelling in the ECM, there are still issues that need to be improved. In [26, 27], a single-valued equivalent resistance was adopted to represent the core loss of the PMSM in the per-phase ECM. However, nowadays PMSMs are also widely used in speed-varying situations, and the single-valued equivalent resistance model cannot correctly predict the core loss in a wide speed range. In order to express the core loss changes with the terminal voltage and current of the PMSM, [28, 29] incorporated two single-valued equivalent resistances to describe the voltage-dependent core loss and stator current-

Manuscript received XXX; revised XXX; accepted XXX. Date of publication XXX; data of current version XXX. Recommended by Technical Editor XXX.

Xin Ba, Zhenjie Gong and Chengning Zhang are with the National Engineering Research Center of Electric Vehicles, Beijing Institute of Technology, Beijing 100081, China (email: xin.ba@bit.edu.cn; 7520220170@bit.edu.cn; mrzhchn@bit.edu.cn).

Xiaodong Sun is with the Automotive Engineering Research Institute, Jiangsu University, Zhenjiang 212013, China (email: xdsun@ujs.edu.cn).

Youguang Guo is with School of Electrical and Data Engineering, University of Technology Sydney, NSW 2007, Australia, (email: Youguang.Guo-1@uts.edu.au).

Jian Guo Zhu is with the School of Electrical and Information Engineering, The University of Sydney, NSW 2006, Australia, (email: Jianguo.Zhu@sydney.edu.au).

related core loss in the per-phase ECM, respectively. However, the impact of the magnetic saturation effect on the core loss is neglected in them. [30] modeled the core loss of the PMSM in the per-phase ECM via a variable equivalent resistance, which is a function of the motor speed. This method achieves high performance prediction accuracy in a wide speed range, but the performance prediction error will increase when the motor operates with large stator currents.

This study proposes a generalized per-phase ECM of the PMSM considering the core loss and magnetic saturation effect, and the experiments of a PM TFSM have validated the effeteness and high precision of the proposed method. The main novel contributions of this study are as follows: firstly, three variable equivalent resistances are introduced in the ECM to respectively represent the hysteresis loss, eddy current loss, and anomalous loss, which enable the accurate analysis of the speed-relevant core loss components. Secondly, since only the PM flux contributes to the no-load core loss and induces the back *emf*, no-load core loss equivalent resistances are connected in parallel with the back *emf* only, which are connected in parallel with both the back *emf* and synchronous inductance traditionally. Thirdly, the additional core loss, which is caused by the stator currents, is modelled by a variable resistance, and it is connected in parallel with the synchronous inductance considering the magnetic saturation effect.

The rest parts of this paper are arranged as the following. In Section II, the alternating and rotational core loss are introduced, and then how to model the core loss into the equivalent circuit is developed. Section III proposes a generalized per-phase ECM with predictable core loss, which can predict the core loss under various speeds and loads accurately. Section IV describes the determination of the equivalent core loss resistance, which is crucial for the ECM establishment. In Section V, performance comparisons of ECMs with predictable core loss are presented, and then the discussion and conclusion are drawn in Section VI.

II. Understanding of the Core Loss and Modelling in Equivalent Circuit

Core loss in the PMSM is caused by the alternating magnetic flux, of which only the magnitude varies with time, and rotational magnetic flux, of which both the magnitude and direction of the magnetic flux vary with time. Fig. 1 illustrates the trajectories of the magnetic flux density vectors in the stator core of a PMSM [31]. In the stator yoke and tooth bodies, alternating and elliptical trajectories of the flux density vector can be observed, and the elliptical trajectories are the most common mode of the rotational magnetic field. In the tooth tips, the trajectories are circular approximately, whereas they are rhombic in the tooth roots. The reason of rhombic trajectories is that the magnetic flux density contains high-order harmonics. Therefore, according to the flux density vectors in the PMSM, the core loss can be divided into alternating core loss and rotational core loss, and their mechanisms and mathematical models are completely different. Each kind of core loss consists of three parts: hysteresis loss, eddy current loss, and anomalous loss.

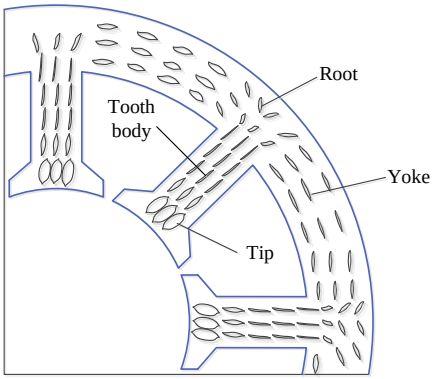

Fig. 1. Trajectories of the flux density vectors in the stator core [31].

For further understanding the difference of the alternating core loss and rotational core loss, Fig. 2 demonstrates the rotational and alternating hysteresis loss of two kinds of ferromagnetic materials obtained by Baily [32]. The alternating hysteresis loss of two kinds of ferromagnetic materials, soft iron and hard steel, grows continuously with the increase of the magnetic flux density. However, for a range of flux density up to about 70% of the saturation value, the rotational hysteresis loss increases with the flux density and is larger than the alternating hysteresis loss. When the flux density continually rises, the rotational hysteresis loss drops dramatically and even vanishes when the flux density reaches the saturation value.

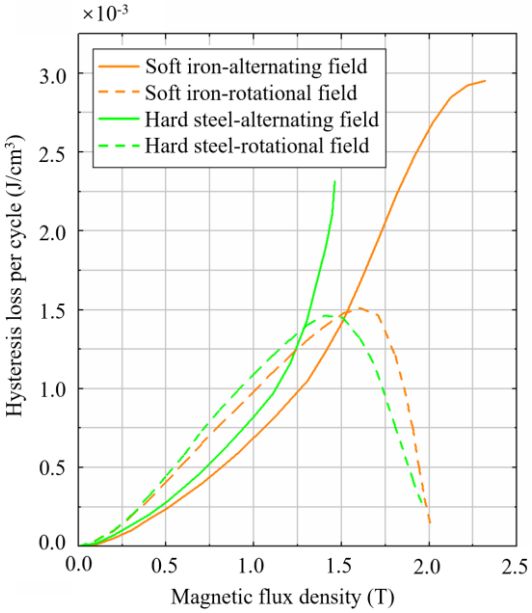

Fig. 2. Rotational and alternating hysteresis loss of iron and steel [32].

The general practice for computing the alternating core loss P_a is based on the three-term model [33-37]

$$P_a = C_{ha} f B_p^h + C_{ea} (f B_p)^2 + C_{aa} (f B_p)^{1.5} \quad (1)$$

The three terms in the right side represents respectively the hysteresis, eddy current, and anomalous loss items, where f and B_P are the flux density frequency and peak value, and the remaining four parameters are all coefficients depending on material properties.

The rotational core loss may be quite different from that with the alternating counterpart, particularly the hysteresis loss component. Some models have been developed and applied, and one example with high-accuracy is shown below [36-39].

$$P_r = P_{hr} + C_{er}(fB_P)^2 + C_{ar}(fB_p)^{1.5} \tag{2}$$

$$\frac{P_{hr}}{f} = a_1\left[\frac{1/s}{(a_2+1/s)^2+a_3^2} - \frac{1/(2-s)}{[a_2+1/(2-s)]^2+a_3^2}\right] \tag{3}$$

$$s = 1 - \frac{B_P}{B_s}\sqrt{1-\frac{1}{a_2^2+a_3^2}} \tag{4}$$

where P_r is the rotational core loss, B_P the peak value of the circularly rotating B vector, B_s is the saturation value of flux density, and the remaining five parameters are all coefficients.

Although there are significant distinctions in the mathematical models of the alternating core loss and rotational core loss, some commonalities still can be extracted. The hysteresis loss is related to the first power of the flux density frequency or rotor speed, the eddy current loss is proportional to the square of the frequency, and the anomalous loss is associated to the 1.5th power of the frequency, and the following equation can be concluded

$$P_c = P_h + P_e + P_{an} = k_h n + k_e n^2 + k_{an} n^{1.5} \tag{5}$$

where P_c is the core loss, n is the speed, and k_h, k_e, and k_{an} are core loss coefficients in the hysteresis, eddy current, and anomalous loss items, respectively.

In order to model the core loss into the equivalent circuit, the most essential issue is to identify and build the relationship between the magnetic field and circuit in the context of the electrical motor. A profound investigation of the mathematical models of the core loss reveals that there are three main factors that affect the core loss, i.e., magnetic properties of materials, flux density frequency, and flux density vectors. A reasonable and practicable ECM with predictable core loss should include these three factors in consideration.

ECM with predictable core loss has not been limited to a standard topology, since the mechanism of the core loss are still not fully understood, hence its modeling in the ECM is also a pending issue. Some topologies have been developed over the last decades to achieve specific features, and the most widely used per-phase ECM of the PMSM is as shown in Fig. 3.

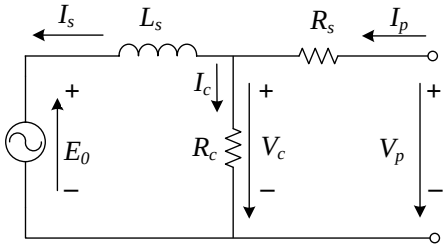

Fig. 3. Per-phase ECM of the PMSM with predictable core loss [30].

In Fig. 3, the equivalent core loss resistance R_c is connected in parallel with the series branch of synchronous inductance L_s and back EMF E_0. If the PMSM is operated with the optimal brushless dc control, i.e., adjusting the armature current I_s and the back *emf* to have the same phase angle, and the terminal voltage V_p is controlled to vary against the back *emf* (or speed) and load current by

$$V_p = E_0 + \mathrm{j}X_s I_s + R_s\left(I_s + \frac{E_0 + \mathrm{j}X_s I_s}{R_c}\right) \tag{6}$$

where R_s is the phase winding resistance, $X_s=\omega_e L_s$ the synchronous reactance, and ω_e is the rotor speed in electrical angular frequency.

The core loss is calculated by

$$P_c = 3\frac{V_c^2}{R_c} = 3\frac{E_0^2 + (X_s I_s)^2}{R_c} \tag{7}$$

To further understand the core loss and the magnetic flux in stator core which arises the core loss, Fig. 4 illustrates the magnetic flux density versus the phase current (root mean square value) in the stator core of the PMSM. When the PMSM operates under the no-load conditions where no current flows in the armature windings, I_p=0, the magnetic flux density in the stator core which generated by PMs is at the inflection point of the magnetization curve, B_{PM}, which closes to the saturation value B_S. When the PMSM operates under the load conditions where there are armature currents fed in the motor, the magnetic flux density in the stator core is the resultant flux density generated by both PMs and phases currents, and it increases slowly with the significant grow of the phase current. Even if the phase current reaches the rated value I_N, the stator core flux density B_N is just much close to the saturation value B_S., and will not increase significant, and that is the magnetic saturation effect. On the other hand, the core loss of the PMSM positively correlates the magnetic flux density. Similar to the relationship of magnetic flux density versus the phase current, the core loss will not increase evidently with the growing phase current.

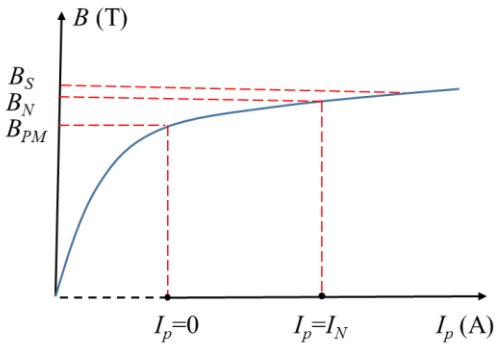

Fig. 4. Magnetic flux density versus the phase current (root mean square value) in the stator core of the PMSM.

Therefore, (7) may much overestimate the extra core loss caused by the armature current. The core loss does go up when the load or armature current increases, but it will not increase so much due to magnetic saturation effect. For example, if the voltage generated by the armature current, X_sI_s, has the same value of E_0, the calculated core loss will be doubled compared with that at no-load conditions where X_sI_s equals zero.

In conclusion, the ECM as shown in Fig. 3 cannot provide accurate core loss predictions, especially when the motor is operating with large loads or armature currents.

III. Proposed Generalized Per-phase ECM with Predictable Core Loss

The proposed generalized per-phase ECM of the PMSM considering the core loss is as shown in Fig. 5. When the PMSM operates at no-load condition, i.e., the armature terminals are open-circuited and hence no current flows in the armature windings, the magnetic flux in the motor is generated by the PMs only. The PM magnetic flux not only contributes the back electromotive force but also causes the core loss; therefore, the equivalent resistance which stands for the no-load core loss should be connected in parallel with the back electromotive force E_0. Since there are three components of the core loss, three equivalent resistances R_h, R_e and R_{an} are adopted to respectively present the hysteresis loss, eddy current loss and anomalous loss at no-load conditions. Various stator core materials have different proportions and development trends of these three core loss components. The advantage of using three resistances rather than single resistance as in the traditional topology is that it makes the core loss evaluation, optimization and even control more flexible and targetable.

When the PMSM operates at loading conditions, i.e., the load current flows in the armature windings, the magnetic flux in the motor is the resultant flux of the PMs-generated flux and the load current-generated flux. Moreover, the magnetic flux in the motor cannot increase linearly with the load current due to the magnetic saturation effect of the stator core. To depict the extra core loss due to the load current and take the magnetic saturation effect into consideration, an equivalent resistance R_i connected in parallel with the synchronous inductance L_s is adopted. The sum of the power loss in R_i, R_h, R_e and R_{an} represents the core loss when the PMSM operates at loading conditions.

Although the proposed ECM is the per-phase model and the input variable is the per-phase current, the magnetic flux density in the stator core is the resultant flux of PMs and all three-phase balanced alternating currents. The flux linkage due to the three-phase balanced alternating currents, which have the relationship of $i_a+i_b+i_c=0$ at any instant, is indicated by the synchronous inductance L_s, and we have the relationship of $L_s=3L_{aa}/2+L_{al}$, where L_{aa} is the self-inductance of per-phase, and L_{al} is the leakage inductance of per-phase.

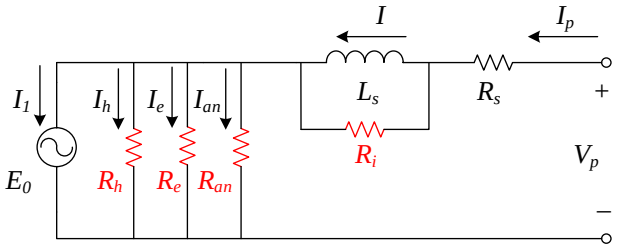

Fig. 5. Generalized per-phase ECM of the PMSM with predictable core loss (In motor convention).

According to the proposed ECM, the mathematical models of the PMSM should be rewritten as

$$\begin{aligned} V_p &= E_0 + R_s I_p + \frac{\mathrm{j}X_s R_i}{\mathrm{j}X_s + R_i} I_p \\ &= E_0 + R_s I_p + \frac{X_s^2 R_i}{X_s^2 + R_i^2} I_p + \frac{\mathrm{j}X_s R_i^2}{X_s^2 + R_i^2} I_p \end{aligned} \tag{8}$$

$$I_p = I_1 + I_h + I_e + I_{an} \tag{9}$$

where V_p and I_p are respectively the phase voltage and phase current. E_0 is the back electromotive force, R_s the phase winding resistance, $X_s=\omega_e L_s$ the synchronous reactance, and R_i, R_h, R_e and R_{an} are equivalent core loss resistances. I_h, I_e, I_{an}, and I_1 are currents flowing through R_h, R_e, R_{an}, and E_0, respectively.

The electromagnetic power and torque of the PMSM can be calculated as

$$P_{em} = n_p E_0 I_1 \cos\psi \tag{10}$$

$$T_{em} = \frac{P_{em}}{\omega_m} \tag{11}$$

where ψ stands for the angle between phasors E_a and I_1, n_p the number of phases, and ω_m is the rotor speed in mechanical angular frequency.

Moreover, the copper loss P_{cu}, the no-load core loss P_{co}, the load core loss P_{ci}, the input power P_{in}, the output power P_{out}, and the efficiency η of the PMSM are obtained as follows

$$P_{cu} = n_p I_p^2 R_s \tag{12}$$

$$P_{co} = P_h + P_e + P_{an} = n_p \frac{E_0^2}{R_h} + n_p \frac{E_0^2}{R_e} + n_p \frac{E_0^2}{R_{an}} \tag{13}$$

$$P_{ci} = P_{co} + P_i = P_h + P_e + P_{an} + P_i = n_p \frac{E_0^2}{R_h} + n_p \frac{E_0^2}{R_e} + n_p \frac{E_0^2}{R_{an}} + n_p I_p^2 \frac{X_s^2 R_i}{X_s^2 + R_i^2} \tag{14}$$

$$P_{in} = n_p V_p I_p \cos\varphi \tag{15}$$

$$P_{out} = P_{em} - P_{mech} \tag{16}$$

$$\eta = P_{out} / P_{in} \times 100\% \tag{17}$$

where φ is the angle between phasors V_p and I_p, n_p the number of phases, and P_{mech} is the mechanical loss of the PMSM.

IV. Determination of the Equivalent Core Loss Resistances

Identification of the parameters in the proposed ECM properly is the key to achieving precise analysis results. Generally, there are two methods to work out these parameters including the equivalent core loss resistances, i.e., the finite element method (FEM) and the experimental test. Three-dimensional core loss calculation considering the rotational magnetic field is highly recommended due to its superior accurateness, and details can be found in [30]. Although experimental tests are able to provide intuitional and reliable solutions, additional auxiliary equipment is needed to separate the core loss and the mechanical loss. For instance, an identical rotor with non-magnetized PMs, or an equivalent stator made of non-ferromagnetic material.

In this paper, a three-phase PM transverse flux synchronous motor with the SMC core is selected as the prototype motor to verify the proposed ECM, and other types of PM synchronous motor, e.g., surface-mounted PMSM, interior PMSM, claw-pole PMSM, axial flux PMSM, also can be described by this proposed ECM. Furthermore, both the single-phase and multi-phase PMSMs can be represented by this proposed ECM. The parameters of the PM TFSM are listed in Table I, and the prototype motor is illustrated in Fig. 6. The outer rotor configuration is introduced in this PM TFSM, and the permanent magnets are mounted on the inner surface of the rotor. The stator has three stacks of core which are arranged axially, and three concentrated coils are embedded in the stator for three phases.

TABLE I
Parameters of the PM TFSM

Parameter	Value
Number of phases	3
Number of poles	20
Rated power	640 W
Rated speed	1800 r/min
Rated torque	3.4 Nm
Rated phase current	5.5 A
Winding resistance	0.41 Ω
Synchronous inductance	6.08 mH
PM flux	0.28 mWb
Number of turns of a phase winding	125

(a) (b)

Fig. 6. Prototype of the PM TFSM: (a) Rotor, (b) Stator.

For determining the equivalent core loss resistance, R_h, R_e and R_{an}, the no-load core loss data should be figured out. In this study, all parameters in the ECM are from experimental tests, and Table II lists the measured no-load core loss with different speed or frequency [15, 19]. The core loss measurement of the PM motor is a complex process and requires additional auxiliary components, such as a dummy rotor or stator, to imitate and measure the mechanical loss of the motor. In this study, the stator of the PM motor is replaced by a wood one to imitate the windage, and hence measure the mechanical loss of the PM motor without the coupled core loss. Drive the PM motor as a generator and select a DC motor as the prime mover, and the armature terminals of the PM motor are open-circuited and hence no current flows in the armature windings, i.e., no copper loss. The electromagnetic properties of the selected DC motor have been well measured in advance. Therefore, the power fed into the DC motor when it drives the PM motor subtracting the power fed into the DC motor when it operates alone yields the total of the core loss and mechanical loss of the PM motor. Then, the total of the core loss and mechanical loss subtracting the mechanical loss of the PM motor, which is measured with the help of the dummy stator, obtains the core loss of the PM motor.

TABLE II
Measured No-load Core Loss of the PM TFSM

Speed (rpm)	Core Loss (W)
200	4.2
400	9.3
600	15.3
800	22.1
1000	29.8
1200	38.4
1400	47.9
1600	58.2
1800	69.4

Notice that the flux density frequency in the stator of the PMSM is proportional to the speed of the PMSM, and then by combining (5) and (13), the no-load core loss of the PM TFSM is obtained as

$$P_c = n_p E_0^2 \left(\frac{1}{R_h} + \frac{1}{R_e} + \frac{1}{R_{an}}\right) = k_h n + k_e n^2 + k_{an} n^{1.5} \tag{18}$$

where n is the speed of the PMSM, n_p=3 for this PM TFSM.

By curve-fitting the data in Table II, the core loss coefficients can be obtained as k_h=1.881×10^{-2} W/rpm, k_e=1.085×10^{-5} W/(rpm)^2, and k_{an}=5.178×10^{-6}. As E_0=4.44$fN\Phi_m$ and f=pn/120, where p=20 is the number of poles, E_0=0.0259n. It can be deduced that R_h is a linear function of motor speed n, R_{an} is proportional to the square root of n, and R_e is a constant. Then we can obtain R_h =0.107n Ω, R_e =185.5 Ω, and R_{an} =388.7$\sqrt{n}$ Ω.

For determining R_i, the motor core loss under various load currents should be figured out. It should be noted that the motor control method will affect the magnetic field distribution and hence the core loss. Here, the PM TFSM is driven by the so-called optimal brushless dc control, i.e., the armature current is controlled to be in phase with the back *emf*, so I_p lags Φ_m by 90 degrees.

Actually, the synchronous reactance is a function of the motor speed as well

$$X_s = \frac{\pi p L_s}{60} n \tag{19}$$

where p is the number of poles, and n is the motor speed.

Substitute (13) and (19) into (14) and solve it, and R_i can be obtained as

$$R_i = \frac{S_2^2 n^2 + S_2 n\sqrt{S_2^2 n^2 - 4S_1^2}}{2S_1} \tag{20}$$

where

$$S_1 = \frac{P_{ci} - P_{co}}{n_p I_p^2} \tag{21}$$

$$S_2 = \frac{\pi p L_s}{60} \tag{22}$$

The core loss of the PM TFSM at the rated speed 1800 rpm and rated load current 5.5 A is 120.3 W, and from the above-mentioned equations, S_1=0.56 and S_2=6.37×10^{-3}. Therefore, the equivalent resistance R_i for the PM TFSM is computed as

$$R_i = \frac{(6.37\times10^{-3})^2 n^2 + (6.37\times10^{-3}) n\sqrt{(6.37\times10^{-3})^2 n^2 - 1.2544}}{1.12} \tag{23}$$

V. Performance Comparisons of ECMs with Predictable Core Loss

There are two vital points that determine the accuracy of the ECMs with predictable core loss. The first is where the equivalent core loss resistance should be placed, and the second is how to identify the value of the equivalent core loss resistance. Through a comprehensive and in-depth analysis of the previous literature [40], two representative methods will be used to compare with the proposed method in this paper.

Method 1: the topology of the ECM is as shown in Fig. 3, and the equivalent core loss resistance R_c is a single-valued resistance and determined based on the core loss at rated speed and no-load condition. For the PM TFSM, R_c=94 Ω.

Method 2: the topology of the ECM is as shown in Fig. 3, and the equivalent core loss resistance R_c is a function of the motor speed and determined based on the no-load core loss at various speeds. For the PM TFSM, R_c=0.0583n Ω, where n is the motor speed.

The experimental platform of the PM TFSM is illustrated in Fig. 7. It mainly contains a DC motor, a torque transducer, and the PM TFSM with SMC core. These two motors are connected via a torque transducer, and both of them can operate as the driver or load, depending on performance testing requirements. The torque transducer was made in Switzerland, and the type is Vibrometer TM109 S/N 0148, and the range is 20 Nm. The torque transducer has been calibrated before the test to guarantee the accuracy of the measurement. More conveniently, the neutral point of the three phase windings is led to outside for measurement.

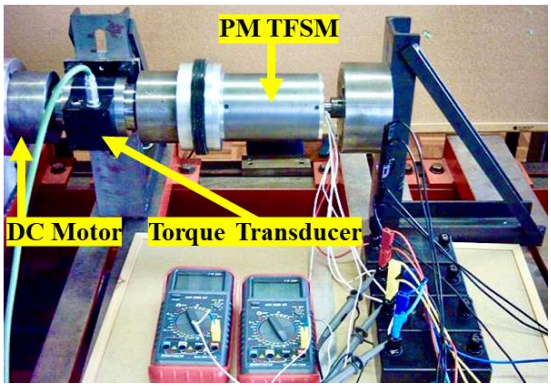

Fig. 7. Experimental platform of the PM TFSM with SMC core.

Fig. 8 demonstrates the predicted no-load core loss via method 1, method 2, the proposed method, and measured core loss. It can be seen that the proposed method can predict the no-load core loss with the highest precision, followed by method 2, while method 1 has the lowest precision.

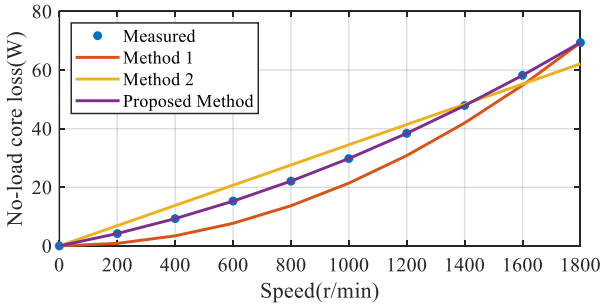

Fig. 8. No-load core loss versus motor speed predicted by different methods.

The errors between the measured no-load core loss and predicted values are evaluated via the standard deviation, and that is calculated as

$$\sigma = \sqrt{\frac{1}{N}\sum_{i=1}^{N}(x_i - \bar{x})^2} \tag{24}$$

The standard deviation of method 1 is about 6.22, and that of method 2 is 4.88, while that of the proposed method is close to zero. Quantitative analysis confirms that the proposed ECM and parameter identification method have superior performance in core loss prediction.

Another distinctive merit of the proposed ECM is that it makes the analysis of each component of core loss possible, and the hysteresis loss, eddy current loss, and anomalous loss versus motor speed are depicted in Fig. 9. In the motor speed range of 0 to 1750 r/min, the hysteresis loss dominates the core loss, while the eddy current loss will master the core loss in the higher speed range, and the anomalous loss, which is less than 1 W even at the rated speed of 1800 r/min, maintains the lowest value.

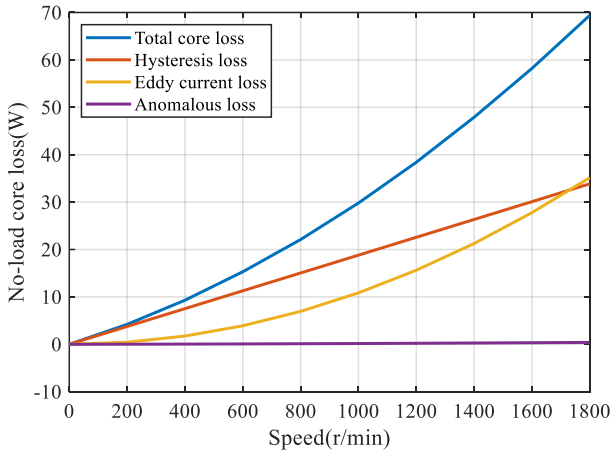

Fig. 9. No-load core loss and its components versus motor speed.

Furthermore, the proposed ECM has significant advantages in predicting the core loss and performance under loading conditions. Fig. 10 presents the core loss at the rated operating point predicted by different methods, at which the phase current is 5.5 A and the motor speed is 1800 r/min. Due to the ignoring of the magnetic saturation effect, methods 1 and 2 notably overestimate the core loss, but the proposed method can estimate it accurately.

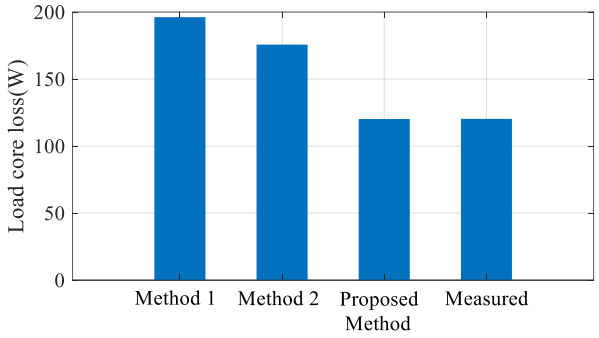

Fig. 10. Core loss at the rated operating point predicted by different methods.

An excellent ECM with predictable core loss of the PMSM is not only able to predict the core loss correctly, but also can predict the output performance of the motor reliably. Since the measurement of the load core loss is very difficult and hard to ensure accuracy, and we need to separate the output power, copper loss and mechanical loss from the input power, we compare the mechanical characteristics and efficiency of the motor which includes the calculation and comparison of the load core loss in following paragraphs.

When the PM TFSM operates under the optimal brushless dc control with a dc link voltage, i.e., adjusting the current I_1 and back *emf* E_0 to have the same phase angle, the phase voltage of the motor can be obtained as

$$V_p = \sqrt{(E_0 + R_s I_p + \frac{I_p X_s^2 R_i}{X_s^2 + R_i^2})^2 + (\frac{I_p X_s R_i^2}{X_s^2 + R_i^2})^2} \tag{25}$$

Therefore, the mechanical characteristic of the PM TFSM, i.e., the relation of the motor speed and output torque can be worked out from (25) as

$$\begin{aligned} V_p^2 = &\left[k_{emf} n + R_s (\frac{T_{em}}{k_T} + \frac{k_{emf}}{k_h} + \frac{k_{emf} n}{k_e} + \frac{k_{emf}\sqrt{n}}{k_{an}}) \right. \\ &\left. + \frac{k_{Xs}^2 n^2 R_i}{k_{Xs}^2 n^2 + R_i^2} (\frac{T_{em}}{k_T} + \frac{k_{emf}}{k_h} + \frac{k_{emf} n}{k_e} + \frac{k_{emf}\sqrt{n}}{k_{an}}) \right]^2 \\ &+ \left[\frac{k_{Xs} n R_i^2}{k_{Xs}^2 n^2 + R_i^2} (\frac{T_{em}}{k_T} + \frac{k_{emf}}{k_h} + \frac{k_{emf} n}{k_e} + \frac{k_{emf}\sqrt{n}}{k_{an}}) \right]^2 \end{aligned} \tag{26}$$

where k_{emf}=0.0259 V/rpm is the back *emf* constant, $k_{Xs}=2\pi p L_s/120$=0.00637 Ω/rpm is the synchronous reactance constant, and $k_T=90k_{emf}/\pi$=0.742 Nm/A is the electromagnetic torque constant.

In methods 1 and 2, the phase voltage equation can be obtained by rewriting (6) as

$$V_p = \sqrt{(E_0 + R_s I_s + \frac{E_0 R_s}{R_c})^2 + (X_s I_s + \frac{X_s I_s R_s}{R_c})^2} \quad (27)$$

The mechanical characteristic of the PM TFSM can be calculated as

$$V_p^2 = \left[k_{emf} n + R_s \frac{T_{em}}{k_T} + \frac{k_{emf} R_s n}{R_c} \right]^2 + \left[k_{Xs} n \frac{T_{em}}{k_T} (1 + \frac{R_s}{R_c}) \right]^2 \quad (28)$$

To furtherly demonstrate the superiority of the ECM considering the core loss, the ECM ignoring the core loss is also be compared, and hence the voltage equation becomes

$$V_p = E_0 + R_s I_p + \mathrm{j} X_s I_p \quad (29)$$

where the currents passing through E_0, R_s and X_s are the same. As I_p is controlled to be in phase with E_0, one can obtain

$$V_p^2 = (k_{emf} n + R_s \frac{T_{em}}{k_T})^2 + (k_{Xs} n \frac{T_{em}}{k_T})^2 \quad (30)$$

For V_{dc}=192 V, the curves of the mechanical characteristic in terms of the motor speed against output torque are solved by different methods as shown in Fig. 11. It is noted from the prototype experiment that the ratio of V_p over V_{dc} is not fixed, but decreases by a slope of approximately 10% against the increase of torque. In order to have a fair comparison with the measured data, this variation is included in the prediction of the mechanical characteristics.

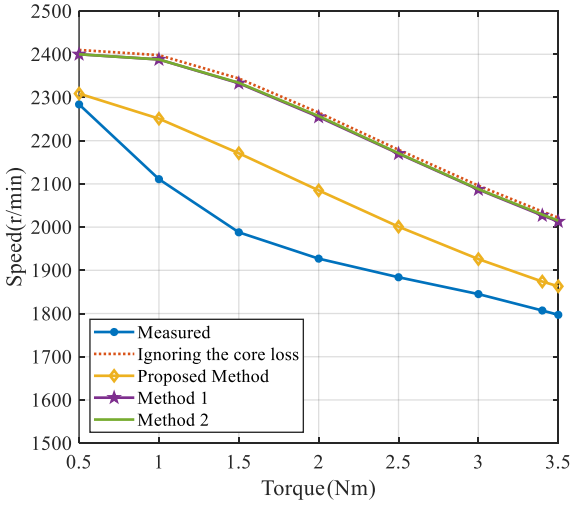

Fig. 11. Mechanical characteristics of the motor predicted by different methods.

It is seen from the figure that the prediction of ignoring the core loss is far from the measurement, while method 1 and method 2 can improve the predicted results slightly. Compared with these counterparts, the proposed method has the best performance in predicting the mechanical characteristic of the PMSM. This comparison results indirectly verify the superiority of the proposed method in predicting the load core loss of the motor.

To quantitatively compare the four cases, their errors are calculated. It is seen that the predicted speeds when ignoring the core loss have an average error of 13.6% compared to the measurements, while the average errors marginally decrease to 13.13% and 13.19% in method 1 and method 2 respectively, and it decreases considerably to 5.4% in the proposed method.

The most notable advantage of the ECM, compared to the finite element method, can provide various analysis results with much less calculation burden. An example of applying the proposed ECM to analyse the motor efficiency is constructed, as shown in Fig. 12. In the optimal brushless dc control mode, the maximum efficiency of the PM TFSM is 80%, which is consistent with the prototype measurement.

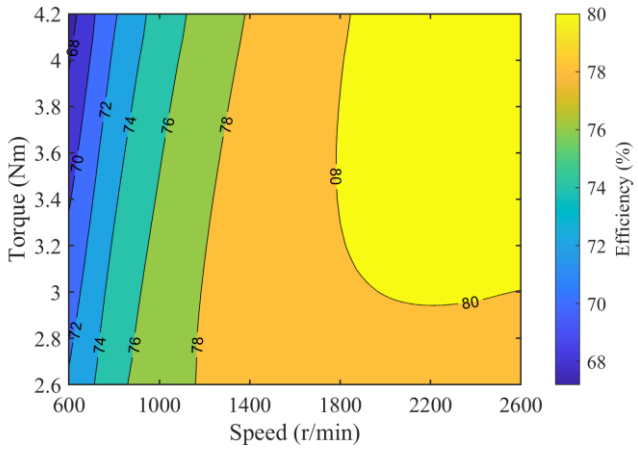

Fig. 12. Efficiency map of the PM TFSM.

VI. Discussion and Conclusion

This paper presented a generalized per-phase equivalent circuit model with predictable core loss, for predicting the core loss and analyzing the performance of PMSMs under varying speed and load conditions. The proposed model has been applied to calculate the performance of a PM transverse flux synchronous motor under the optimal brushless dc control mode. Compared with previous studies of the ECMs with predictable core loss, the proposed method has better accuracy in both no-load and load core loss predictions, and can analyze the hysteresis loss, eddy current loss, and anomalous loss separately. Furthermore, in predicting the motor performance, such as mechanical characteristics, the proposed method can provide more reliable results compared to the traditional ECM ignoring the core loss as well as previous ECMs considering

core loss. The superior performances of the proposed method have been verified by experiments.

The proposed model of the PMSM can be versatilely used in motor design, optimization, and control with fast calculation speed. For example, the developed model is also be useful for improving the performance of the PMSM under other motor control strategies such as model predictive control, in which the mathematical model will be more accurate by considering the core loss under varying speed and load conditions.

Finally, a brief discussion about whether the eddy current loss of PMs should be included in the ECM is launched. The ECM of the synchronous motor is different from that of the asynchronous motor. To be more specific, in the ECM of the asynchronous motor, the electromagnetic parameters of the rotor, such as the rotor winding resistance, are included. By contrast, in the ECM of the synchronous motor, the electromagnetic parameters of the rotor are eliminated since the stator and rotor of it are rotating at the same speed. Generally, eddy current loss in PMs is a part of loss which occurs in the rotor, and electromagnetic characteristics of the rotor are excluded in the ECM of the synchronous motor. Therefore, authors of this paper think that modelling the eddy current loss of PMs in the ECM of the synchronous motor is less theoretical supports.

REFERENCES

[1] S. Hu, M. Xiong, Z. Liang, and X. He, "Torque distributed control strategy for the dual three-phase PMSM in hybrid energy storage system application," *IEEE Trans. Ind. Electron.*, vol. 67, no. 4, pp. 2544-2552, 2020.

[2] Z. Gong, C. Zhang, X. Ba and Y. Guo, "Improved deadbeat predictive current control of permanent magnet synchronous motor using a novel stator current and disturbance observer," *IEEE Access*, vol. 9, pp. 142815-142826, 2021.

[3] C. Calleja, A. Lopez-de-Heredia, H. Gaztanaga, and T. Nieva, "Validation of a modified direct-self-control strategy for PMSM in railway-traction applications," *IEEE Trans. Ind. Electron.*, vol. 63, no. 8, pp. 5143-5155, 2016.

[4] K. K. Prabhakaran, A. Karthikeyan, B. V. Perumal, and S. Mishra, "Standalone single stage PV-fed reduced switch inverter based PMSM for water pumping application," *IEEE Trans. Ind. Appl.*, vol. 56, no. 6, pp. 6526-6535, 2020.

[5] Y. Ma, D. Li, Y. Li and L. Yang, "A novel discrete compound integral terminal sliding mode control with disturbance compensation for PMSM speed system," *IEEE/ASME Trans. Mechatronics*, vol. 27, no. 1, pp. 549-560, 2022.

[6] K. Zhao *et al*., "Demagnetization-fault reconstruction and tolerant-control for PMSM using improved SMO-based equivalent-input-disturbance approach," *IEEE/ASME Trans. Mechatronics*, vol. 27, no. 2, pp. 701-712, 2022.

[7] K. T. Chau, C. C. Chan, and C. Liu, "Overview of permanent magnet brushless drives for electric and hybrid electric vehicles," *IEEE Trans. Ind. Electron.*, vol. 55, no. 6, pp. 2246-2257, 2008.

[8] Z. Q. Zhu and D. Howe, "Electrical machines and drives for electric, hybrid, and fuel cell vehicles," *Proc. of the IEEE*, vol. 95, no. 4, pp. 746-765, 2007.

[9] X. Sun, Z. Shi, Y. Cai, G. Lei, Y. Guo, and J. G. Zhu, "Driving-cycle-oriented design optimization of a permanent magnet hub motor drive system for a four-wheel-drive electric vehicle," *IEEE Trans. Electrificat.*, vol. 6, no. 3, pp. 1115-1125, 2020.

[10] A. Bosso, C. Conficoni, D. Raggini and A. Tilli, "A computational-effective field-oriented control strategy for accurate and efficient electric propulsion of unmanned aerial vehicles," *IEEE/ASME Trans. Mechatronics*, vol. 26, no. 3, pp. 1501-1511, 2021.

[11] X. Yang, B. Kou, J. Luo, and H. Zhang, "A novel dual-consequent-pole transverse flux motor and its analytical modeling," *IEEE Trans. Ind. Electron.*, vol. 68, no. 5, pp. 4141-4152, 2021.

[12] X. Zhao and S. Niu, "Development of a novel transverse flux tubular linear machine with parallel and complementary PM magnetic circuit for precision industrial processing," *IEEE Trans. Ind. Electron.*, vol. 66, no. 6, pp. 4945-4955, 2019.

[13] M. Wang, P. Zheng, C. Tong, Q. Zhao, and G. Qiao, "Research on a transverse-flux brushless double-rotor machine for hybrid electric vehicles," *IEEE Trans. Ind. Electron.*, vol. 66, no. 2, pp. 1032-1043, 2019.

[14] J. Doering, G. Steinborn, and W. Hofmann, "Torque, power, losses, and heat calculation of a transverse flux reluctance machine with soft magnetic composite materials and disk-shaped rotor," *IEEE Trans. Ind. Appl.*, vol. 51, no. 2, pp. 1494-1504, 2015.

[15] Y. Guo, J. G. Zhu, P. A. Watterson, and W. Wu, "Development of a PM transverse flux motor with soft magnetic composite core," *IEEE Trans. Energy Convers.*, vol. 21, no. 2, pp. 426–434, 2006.

[16] T. Ishikawa, Y. Sato, and N. Kurita, "Performance of novel permanent magnet synchronous machines made of soft magnetic composite," *IEEE Trans. Magn.*, vol. 50, no. 11, art. 8105304, 2014.

[17] W. Du, S. Zhao, H. Zhang, M. Zhang, and J. Gao, "A novel claw pole motor with soft magnetic composites," *IEEE Trans. Magn.*, vol. 57, no. 2, art. 8200904, 2021.

[18] Q. Chen, D. Liang, S. Jia, Q. Ze, and Y. Liu, "Analysis of winding MMF and loss for axial PMSM with FSCW layout and YASA topology," *IEEE Trans. Ind. Appl.*, vol. 56, no. 3, pp. 2622-2635, 2020.

[19] Y. Guo, J. G. Zhu, H. Lu, Y. Li, and J. X. Jin, "Core loss computation in a permanent magnet transverse flux motor with rotating fluxes," *IEEE Trans. Magn.*, vol. 50, no. 11, art. 6301004, 2014.

[20] W. Tong, S. Li, R. Sun, L. Sun, and R. Tang, "Modified core loss calculation for high-speed PMSMs with amorphous metal stator cores," *IEEE Trans. Energy Convers.*, vol. 36, no. 1, pp. 560-434, 2021.

[21] X. Liu, G. Liu, and H. Han, "A loss separation method of a high-speed magnetic levitated PMSM based on drag system experiment without torque meter," *IEEE Trans. Ind. Electron.*, vol. 66, no. 4, pp. 2976-2986, 2019.

[22] X. Sun, Y. Zhang, G. Lei, Y. Guo and J. Zhu, "An improved deadbeat predictive stator flux control with reduced-order disturbance observer for in-wheel PMSMs," *IEEE/ASME Trans. Mechatronics*, vol. 27, no. 2, pp. 690-700, 2022.

[23] S. S. Kuruppu and Y. Zou, "Static position sensor bias fault diagnosis in permanent magnet synchronous machines via current estimation," *IEEE/ASME Trans.Mechatronics*, vol. 26, no. 2, pp. 888-896, 2021.

[24] F. Bu *et al*., "Rotor position tracking control for low speed operation of direct-drive PMSM servo system," *IEEE/ASME Trans. Mechatronics*, vol. 26, no. 2, pp. 1129-1139, 2021.

[25] S. K. Kommuri, Y. Park and S. B. Lee, "Online compensation of mechanical load defects with composite control in PMSM drives," *IEEE/ASME Trans. Mechatronics*, vol. 26, no. 3, pp. 1392-1400, 2021.

[26] V. Honsinger, "Performance of polyphase permanent magnet machines," *IEEE Trans. Power App. and Syst.*, vol. PAS-99, no. 4, pp. 1510-1518, 1980.

[27] R. S. Colby and D. W. Novotny, "Efficient operation of surface-mounted PM synchronous motors," *IEEE Trans. Ind. Appl.*, vol. IA-23, no. 6, pp. 1048-1054, 1987.

[28] A. Consoli and G. Renna, "Interior type permanent magnet synchronous motor analysis by equivalent circuits," *IEEE Trans. Energy Convers.*, vol. 4, no. 4, pp. 681-689, 1989.

[29] A. Consoli and A. Raciti, "Analysis of permanent magnet synchronous motors," *IEEE Trans. Ind. Appl.*, vol. 27, no. 2, pp. 350-354, 1991.

[30] X. Ba, Y. Guo, J. G. Zhu, and C. Zhang, "An equivalent circuit model for predicting the core loss in a claw-pole permanent magnet motor with soft magnetic composite core," *IEEE Trans. Magn.*, vol. 54, no. 11, art. 8206706, 2018.

[31] K. Senda, M. Ishida, A. Honda, and I. Ohyama, "Local magnetic properties in operating brushless DC motor," (in Japanese), in *Proc. Papers Tech. Meeting Rotating Mach.*, 2003, Paper RM-03-42, pp. 49–54.

[32] F. G. Baily, "The hysteresis of iron and steel in a rotating magnetic field," *Proc. of the Royal Society of London*, vol. 60, issue 359-367, pp. 182-184, 1897.

[33] D. M. Ionel, M. Poescu, M. I. McGilp, T. J. E. Miller, S. J. Dellinger, and R. J. Heideman, "Computation of core losses in electrical machines using

improved models for laminated steel," *IEEE Trans. Ind. Appl.*, vol. 43, no. 6, pp. 1554-1564, 2007.
[34] M. Ibrahim and P. Pillay, "Advanced testing and modeling of magnetic materials including a new method of core loss separation for electrical machines," *IEEE Trans. Ind. Appl.*, vol. 48, no. 5, pp. 1507-1515, 2012.
[35] M. S. Lim, J. H. Kim, and J. P. Hong, "Experimental characterization of the slinky-laminated core and iron loss analysis of electrical machine," *IEEE Trans. Magn.*, vol. 51, no. 11, art. 8204504, 2015.
[36] Y. Zhang, Y. Liu, Y. Li, D. Xie, and B. Bai, "A complex-valued rotating magnetic property model and its application to iron loss calculation," *IEEE Trans. Magn.*, vol. 50, no. 2, art. 7009704, 2014.
[37] S. Urata, M. Enokizono, T. Todaka, and H. Shimoji, "Magnetic characteristic analysis of the motor considering 2-D vector magnetic property," *IEEE Trans. Magn.*, vol. 42, no. 4, pp. 615-618, 2016.
[38] X. Zhao, H. Xu, Y. Li, L. Zhou, X. Liu, H. Zhao, Y. Liu, and D. Yuan, "Improved Preisach model for vector hysteresis property of soft magnetic composite materials based on the hybrid technique of SA-NMS," *IEEE Trans. Ind. Appl.*, early access, 2021.
[39] Y. Guo, J. G. Zhu, H. Lu, Z. Lin, and Y. Li, "Core loss calculation for soft magnetic composite electrical machines," *IEEE Trans. Magn.*, vol. 48, no. 11, pp. 3112-3115, 2012.
[40] X. Ba, Z. Gong, Y. Guo, C. Zhang, and J. Zhu, "Development of equivalent circuit models of permanent magnet synchronous motors considering core loss," *Energies*, vol. 15, no. 6, p. 1995, Mar. 2022.

Xin Ba received the B.E. degree from Lanzhou University of Technology, Lanzhou, China, in 2011, the M.E. degree from Beijing Information Science and Technology University, Beijing, China, in 2015, and the Ph.D. degree from Beijing Institute of Technology, China, in 2020, all in mechanical engineering.

She is currently a PhD candidate in electrical engineering at the School of Electrical and Data Engineering, University of Technology Sydney, Australia, and a postdoctoral fellow at school of mechanical engineering, Beijing Institute of Technology, China. Her research interests include measurement and modelling of properties of magnetic materials, and numerical analysis of electromagnetic field.

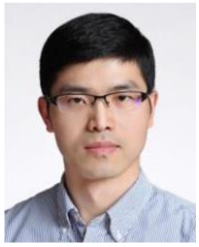

Xiaodong Sun (Senior member, IEEE) received the B.Sc. degree in electrical engineering, and M.Sc. and Ph.D. degrees in control engineering from Jiangsu University, Zhenjiang, China, in 2004, 2008, and 2011, respectively.

Since 2004, he has been with Jiangsu University, where he is currently a Professor in vehicle engineering with the Automotive Engineering Research Institute. From 2014 to 2015, he was a Visiting Professor with the School of Electrical, Mechanical, and Mechatronic Systems, University of Technology Sydney, Sydney, NSW, Australia. He has authored or coauthored more than 100 refereed technical papers and one book, and he is the holder of 42 patents in his areas of interest. His research interests include electrified vehicles, electrical machines, electrical drives, and energy management.

Prof. Sun is an Editor of the IEEE Transactions on Energy Conversion.

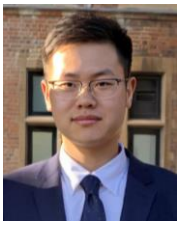

Zhenjie Gong received the B.E. degree in automation from Inner Mongolia University of Technology, China in 2014, the M.E. degree in electrical engineering from Beijing Information Science and Technology University, China in 2018, and the Ph.D. degree in mechanical engineering from Beijing Institute of Technology, China, in 2022.

He is currently a postdoctoral fellow at school of mechanical engineering, Beijing Institute of Technology, China. His research fields include study on high precision of synchronous motor, power electronic drives and control.

Youguang Guo (Senior member, IEEE) received the B.E. degree from Huazhong University of Science and Technology, China in 1985, the M.E. degree from Zhejiang University, China in 1988, and the Ph.D. degree from University of Technology, Sydney (UTS), Australia in 2004, all in electrical engineering.

He is currently a Professor in Electrical Engineering at the School of Electrical and Data Engineering, University of Technology Sydney (UTS). His research fields include measurement and modeling of properties of magnetic materials, numerical analysis of electromagnetic field, electrical machine design optimization, power electronic drives and control.

Chengning Zhang received the M.E. degree in control theory and control engineering and the Ph.D. degree in vehicle engineering from the Beijing Institute of Technology, Beijing, China, in 1989 and 2001, respectively.

He is currently a Professor of the National Engineering Laboratory for Electric Vehicles, Beijing Institute of Technology. His research interests include electric vehicles, vehicular electric motor drive systems, battery management systems, and chargers

Jianguo Zhu (Senior member, IEEE) received the B.E. degree from Jiangsu Insitute of Technology, Jiangsu, China, in 1982, the M.E. degree from Shanghai University of Technology, Shanghai, China, in 1987, and the Ph.D. degree from the University of Technology Sydney, Sydney, NSW, Australia, in 1995, all in electrical engineering.

He was appointed a Lecturer with the UTS in 1994 and promoted to Full Professor, in 2004, and Distinguished Professor of electrical engineering, in 2017. At the UTS, he has held various leadership positions, including the Head of School for School of Electrical, Mechanical and Mechatronic Systems and Director of Centre for Electrical Machines and Power Electronics. In 2018, he joined the University of Sydney,

Sydney, NSW, Australia, as a Full Professor and the Head of School for School of Electrical and Information Engineering. His research interests include computational electromagnetics, measurement and modeling of magnetic properties of materials, electrical machines and drives, power electronics, renewable energy systems, and smart microgrids.